Materials Today: Proceedings 56 (2022) 3747–3754

Contents lists available at ScienceDirect

Materials Today: Proceedings

journal homepage: www.elsevier.com/locate/matpr

Ruddlesden-Popper phase materials for solid oxide fuel cell cathodes: A short review

Mudasir A. Yatoo *, Stephen J. Skinner

Imperial College London, Department of Materials, Faculty of Engineering, Exhibition Road, London SW7 2AZ, United Kingdom

ARTICLE INFO

Article history:
Available online 15 January 2022

Keywords:
Solid oxide fuel cells
Ruddlesden-Popper phases
Structural chemistry
Oxygen transport
Electrochemical performance
Stability

ABSTRACT

In the last couple of decades, researchers have been working on Ruddlesden-Popper phases to realise them as components of solid oxide cells. Ruddlesden-Popper phase materials have been particularly proposed as materials for intermediate temperature solid oxide fuel cells (IT-SOFCs). As such a sizeable literature was produced on Ruddlesden-Popper phases and in this short review we look at these studies with a particular focus on the structural chemistry, oxygen transport and electrical conductivity, electrochemical performance, and stability of these materials under operating conditions. More specifically, the materials have been studied for cathodes and, therefore, we believe a review dedicated to cathode applications of these materials will be beneficial for the community. A brief outlook on the future directions in the field will also be provided.

1. Introduction

The search for new materials is one of the main ways to meet the needs for future energy conversion and storage technologies. Solid oxide fuel cell is one such technology where advancement in materials has proved important, and it is in this context that the search to find better performing materials continues with aim of reducing the temperature of operation down to the intermediate range (600–800 °C) without slowing the oxygen reduction reaction (ORR) kinetics. Currently, a major direction in the field is materials referred to as mixed-ionic electronic conducting (MIEC) oxides. In contrast with the pure electronic conduction materials such as $La_{1-x}Sr_xMnO_{3-\delta}$ (LSM) where the ORR – represented by the air/cathode/electrolyte interface (Fig. 1) – is limited to a very narrow triple phase boundary (TPB) region, MIEC materials allow the system to extend the ORR region beyond the narrow TPB zone to the entire surface and thus increase the efficiency of the cell (Fig. 2) [1,2].

That LSM perovskite has poor bulk oxygen transport properties results in TPB operation mode, thereby limiting reaction to this interface. This is the main reason that materials with sizeable ionic conductivity are sought to extend the effective TPB regions and MIEC materials such as $La_{1-x}Sr_xCo_{1-y}Fe_yO_{3-\delta}$ (LSCF) perform well in that context. For example, $La_{0.6}Sr_{0.4}Co_{0.2}Fe_{0.8}O_{3-\delta}$, the most promising and studied composition of the LSCF family, shows an electronic conductivity of the order of 350 to 250 Scm^{-1} in the temperature range of 600 to 800 °C along with an ionic conductivity of 10^{-2} Scm^{-1} at 800 °C [3,4].

Apart from perovskites such as LSCF discussed above briefly, other material families such as double perovskites and Ruddlesden-Popper phase materials also show mixed conductivity and are being investigated by researchers for their potential as IT-SOFC cathode materials. Double perovskites are derived from the perovskite structure with the general formula $AA'B_2O_{6-\delta}$ where A is a rare-earth cation, A' is an alkaline earth metal cation and B is a transition metal cation. First reported by Taskin *et al.*, these materials have MIEC properties and have thus attracted significant attention from researchers [5,6]. Taskin *et al.* demonstrated the ionic transport of the double perovskite phases by comparing the chemical diffusion coefficient of ordered $GdBaMn_2O_{5+\delta}$ and disordered $Gd_{0.5}Ba_{0.5}MnO_3$ and reported the significantly higher oxygen diffusion coefficient for the ordered double perovskite material [5,6]. This short review will, however, only discuss Ruddlesden-Popper phases in detail and the reader is invited to consult reviews on perovskites and double perovskites published elsewhere [7–9].

Ruddlesden-Popper phases, with the general formula of $A_{n+1}B_nO_{3n+1}$, were first synthesised by S. N. Ruddlesden and P. Popper in

* Corresponding author.
E-mail address: m.yatoo15@alumni.ac.uk (M.A. Yatoo).

https://doi.org/10.1016/j.matpr.2021.12.537

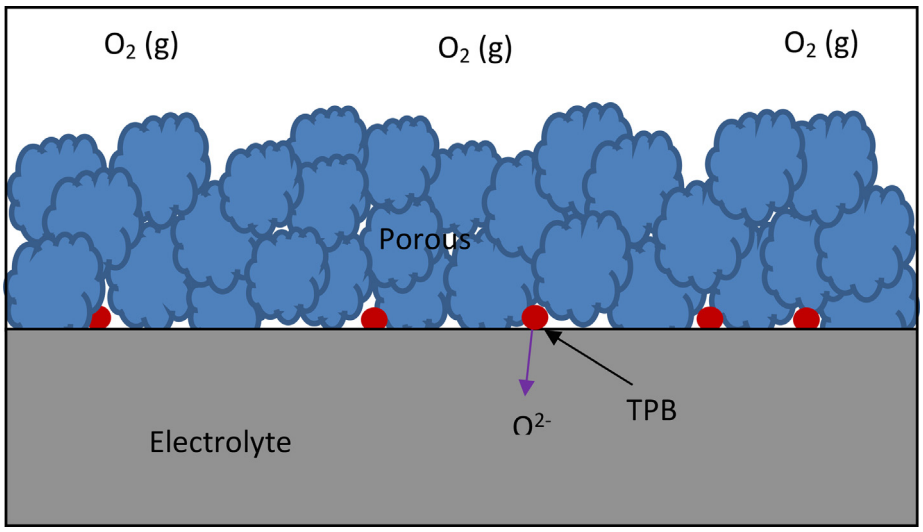

Fig. 1. Schematic representation of three interfaces for ORR. The air/cathode interface, the air/electrolyte interface and air/cathode/electrolyte interface, shown by red dots (reproduced with permission from reference [17]). (For interpretation of the references to colour in this figure legend, the reader is referred to the web version of this article.)

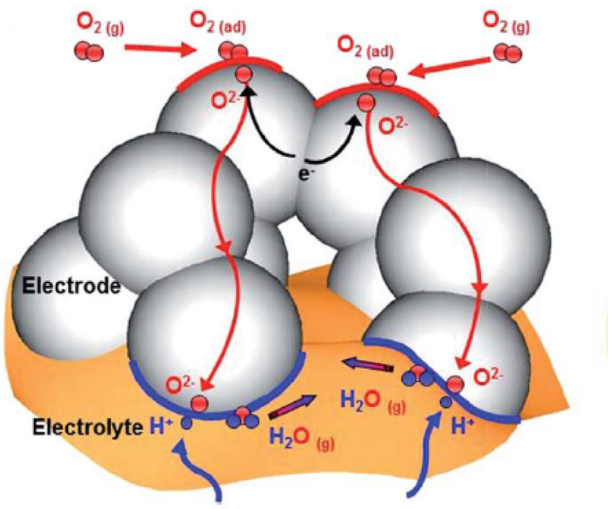

Fig. 2. Schematic representation of the oxygen reaction at MIEC cathode material (reproduced with permission from reference [2]).

1958 [10]. The structure consists of $nABO_3$ perovskite layers which are sandwiched between two AO rock-salt layers [11]. The number of perovskite polyhedral units sandwiched determines the phase of the material (Fig. 3) [12] and this structural similarity of Ruddlesden-Popper phase materials to perovskites is one of the reasons behind the expectation of these materials working as effective SOFC cathodes. The layered structural nature of these materials allows several of them to accommodate a substantial amount of interstitial oxygen. This is because the interstitial sites present in the rock salt AO layers of the Ruddlesden-Popper oxides can accommodate excess oxygen. In addition, the problem of strontium segregation as observed in the state-of-the-art SOFC materials can be avoided because Ruddlesden-Popper phases can be composed of different constituents and do not necessarily contain Sr. In the next sections, we will discuss in detail the structural chemistry and conductivity of these materials and then consider how these materials perform, and comment on their stability under operating conditions.

2. Structural chemistry

The lower-order Ruddlesden-Popper phases such as $La_2NiO_{4+\delta}$ (LNO), $Pr_2NiO_{4+\delta}$ (PNO) and $Nd_2NiO_{4+\delta}$ (NNO) adopt the K_2NiF_4 structure. The La cation is surrounded by nine oxygen atoms and the Ni atoms occupy the centre of apically elongated NiO_6 octahedra with two apical Ni–O bonds along the *c*-axis slightly longer than the other four basal plane Ni–O bonds. Most of the Ruddlesden-Popper phase materials crystallise either in an orthorhombic structure or in a tetragonal structure, which is mostly governed by the value of the Goldschmidt tolerance factor, *t*. When the tolerance factor is closer to unity ($0.99 \geq t \geq 0.88$) the material tends to adopt the higher symmetry tetragonal structure but when the tolerance factor is below 0.88 and lies in the range of $0.88 \geq t \geq 0.865$, the material tends to adopt the lower symmetry orthorhombic structure [13].

The crystal symmetries adopted by a few representative Ruddlesden-Popper phases are provided in Table 1. LNO has been studied extensively and it crystallises in *Fmmm* orthorhombic symmetry, and when A-site La is doped by Pr – as reported by Vibhu *et al.* – La-rich compositions prefer *Fmmm* orthorhombic symmetry while Pr-rich materials lean towards *Bmab* orthorhombic symmetry [14–16]. In some compositions phase transitions to higher symmetry tetragonal *I4/mmm* at higher temperatures have been reported [16].

Higher-order phases too mostly crystallise in orthorhombic symmetry and similar to the transition to tetragonal symmetry at high temperatures, we too in our studies on $La_3PrNi_3O_{10-\delta}$, observed transition to tetragonal *I4/mmm* symmetry at 800 °C [17]. Very recently, Tsai *et al.*, based on their high-resolution neutron powder and X-ray diffraction studies, confirmed that Pr-rich n = 3 phases tend to adopt monoclinic symmetry which we too have observed in $LaPr_3Ni_3O_{10-\delta}$ n = 3 phase [18,19]. It is pertinent to mention that higher-order phases either retain the structural integrity or show no deleterious impact of phase transitions on electrochemical performance at high temperatures which is important for their SOFC applications.

3. Oxygen defects and transport

The main motivation for the intense research focus on the n = 1 Ruddlesden-Popper phase materials stemmed from their superior

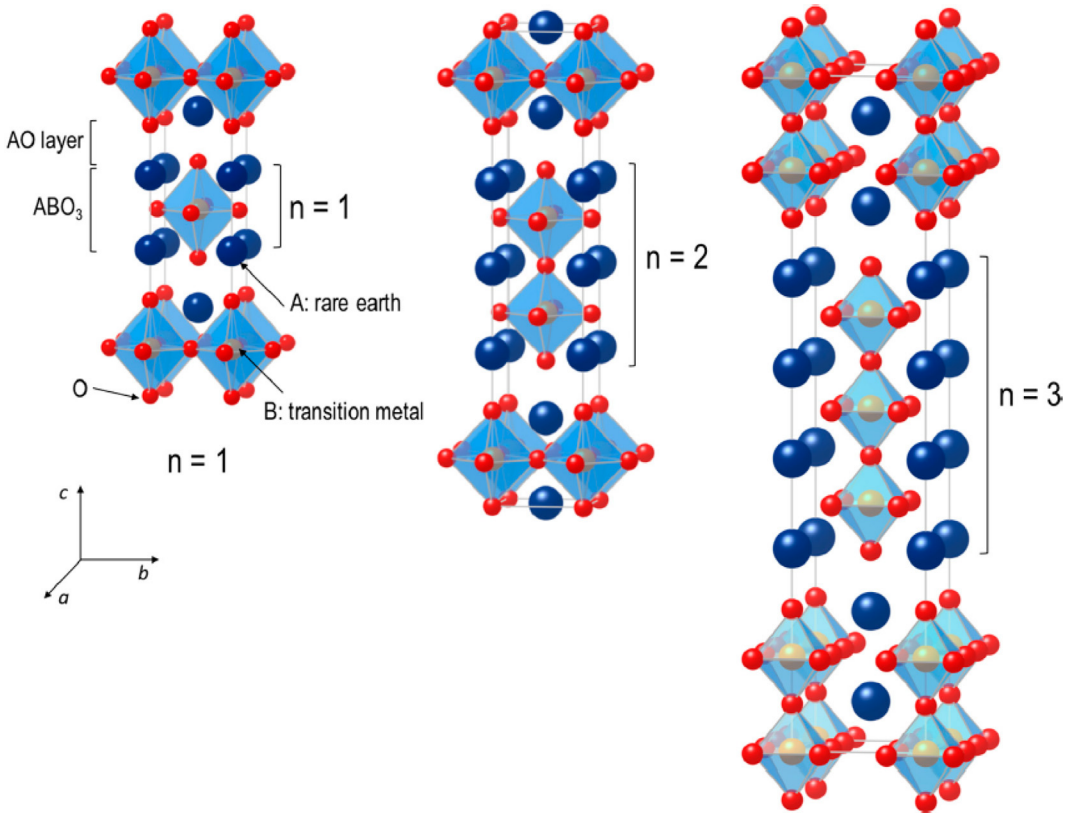

Fig. 3. Simplified illustration of Ruddlesden-Popper phase's structure. The number of perovskite layers sandwiched defines the phase of material (adapted from reference [12]).

Table 1
Crystal symmetry of representative Ruddlesden-Popper phase materials at room temperature.

Composition	Symmetry	Space group	Reference
$La_2NiO_{4+\delta}$	Orthorhombic	*Fmmm*	S. Skinner [14]
$La_{1.75}Pr_{0.25}NiO_{4+\delta}$	Orthorhombic	*Fmmm*	V. Vibhu *et al.* [15]
$La_{0.5}Pr_{1.5}NiO_{4+\delta}$	Orthorhombic	*Bmab*	V. Vibhu *et al.* [15]
$Pr_2NiO_{4+\delta}$	Orthorhombic	*Bmab*	J. M. Bassat *et al.* [16]
$La_3Ni_2O_{7+\delta}$	Orthorhombic	*Fmmm*	G. Amow *et al.* [54]
$La_4Ni_3O_{10-\delta}$	Orthorhombic	*Fmmm*	M. Greenblatt *et al.* [60]
$La_3PrNi_3O_{10-\delta}$	Orthorhombic	*Fmmm*	M. Yatoo *et al.* [70]
$La_2Pr_2Ni_3O_{10-\delta}$	Orthorhombic	*Fmmm*	M. Yatoo *et al.* [69]
$LaPr_3Ni_3O_{10-\delta}$	Monoclinic	$P2_1/a$	M. Yatoo *et al.* [19]
$Pr_4Ni_3O_{10-\delta}$	Monoclinic	$P2_1/a$	C. Y. Tsai *et al.* [18]

capability of storing a substantial amount of interstitial oxygen (Fig. 4) in their structure which bestowed the materials with significant oxide ion conductivity, thereby rendering the materials mixed ionic-electronic conductors (MIEC) at intermediate temperatures [20,21].

The nature of ionic conductivity in these materials has been much debated by researchers. Therefore, detailed studies have been carried out on the LNO material and its transport properties are well understood. There is broad agreement regarding the dominant participation of interstitial oxygen atoms in ionic conductivity [22]. The neutron diffraction studies by Demourgues *et al.* predicted that interstitial oxygen atoms were accommodated by the LaO rock salt layer. This was further confirmed by Jorgensen and co-workers, and they determined the location of the oxygen interstitial site to be at $(\frac{1}{4}\ \frac{1}{4}\ \frac{1}{4})$ in the *Fmmm* structure [23,24]. These studies had further support from Paulus *et al.* who studied single crystals of LNO and confirmed the location of excess oxygen in the rock salt LaO layer, thereby lending further support to the initial studies [25]. In addition, Skinner reported the lengthening of apical Ni–O bonds on heating LNO, a consequence of loss of excess oxygen from interstitial sites located in the La–O plane and therefore lending further support to these earlier studies [14].

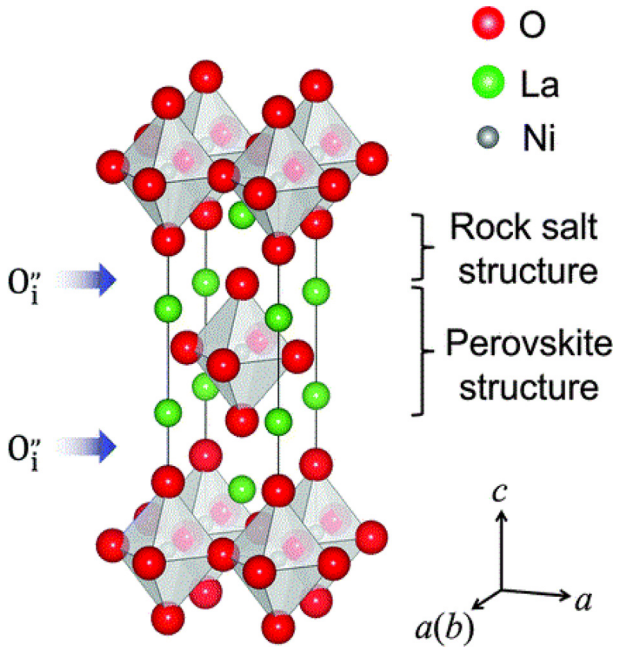

Fig. 4. Schematic of LNO showing the location of interstitial oxygen atoms (reproduced with permission from reference [22]).

To expand the understanding of the role played by oxygen interstitials in ionic conduction properties of $La_2NiO_{4+\delta}$ materials and to also lend further support to experimental evidence, computational studies have been carried out. Computational studies have largely supported the earlier conclusions by several neutron diffraction studies on LNO [26,27], though a debate has emerged between computational studies. Both monovalent and divalent oxygen ions were reported to be involved in interstitialcy transport by Minervini *et al.* whereas more recent density functional theory calculations and atomistic modelling predict only divalent oxygen ions [27–29]. However, both computational approaches have confirmed the interstitialcy mechanism of oxygen transport and are thus in line with experimental studies. Further support was afforded by molecular dynamics simulation performed by Parfitt *et al.* on PNO which showed that oxygen diffusion is highly anisotropic and occurs almost entirely by means of an interstitialcy mechanism in the *a*–*b* plane [30]. It was later further shown experimentally by studies on a related composition by Yashima *et al.* (Fig. 5) [31].

As mentioned earlier it is because of this capability of accommodating a considerable amount of excess oxygen as interstitials in the rock salt layer that the ionic conductivity of n = 1 Ruddlesden-Popper phases materials such as LNO, PNO and NNO surpasses the most promising IT-SOFC perovskite LSCF cathode. Fig. 6 illustrates and compares the ionic conductivity of these lower-order Ruddlesden-Popper phases with LSCF [32].

Participation of both oxygen interstitial species and oxygen vacancies in the ionic conductivity has been reported by experimental studies, with the vacancy activation energy smaller than the interstitial activation energy [20,33]. The prediction of lower activation energy for a process involving oxygen vacancies was confirmed by secondary ion mass spectrometry (SIMS) studies carried out by Bassat and co-workers [32]. Bassat *et al.* further found substantial anisotropy, with conductivity perpendicular to the *a*-*b* plane lower than conductivity parallel to the *a*-*b* plane. This was explained by the fact that oxygen interstitials are confined to LaO rock salt layers and thus contribute towards only parallel conductivity.

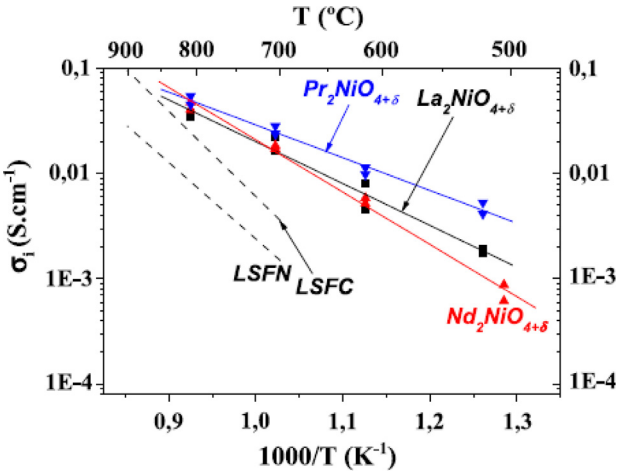

Fig. 6. Comparison of ionic conductivity vs. 1/T best known perovskite-based IT-SOFC cathode materials, LSFC and LSFN (reproduced with permission from reference [32]).

The oxygen diffusion coefficient (D^*) and surface exchange coefficient (k^*) of La, Pr and Nd analogues has been found to be high reflecting the superior ionic conductivity and electrocatalytic properties of these materials [21,34–36]. The diffusion coefficients were measured by Bassat *et al.* and they reported that the PNO shows the highest diffusion coefficient among the nickelates [37]. They also reported that the oxygen diffusion along the *ab*-plane is almost three orders of magnitude higher when compared to the diffusion measured along the *c*-axis. In addition, all the compositions in their polycrystalline forms show even better diffusion, which could possibly mean higher ionic conductivity in the polycrystalline form (Fig. 7) [12,32].

LNO has shown excellent IT-SOFC cathode features [20,21,38]. The oxygen overstoichiometry (+δ) of the material is significant since it is responsible for the superior ionic conductivity, the value of which easily surpasses the state-of-the-art LSCF cathodes in the

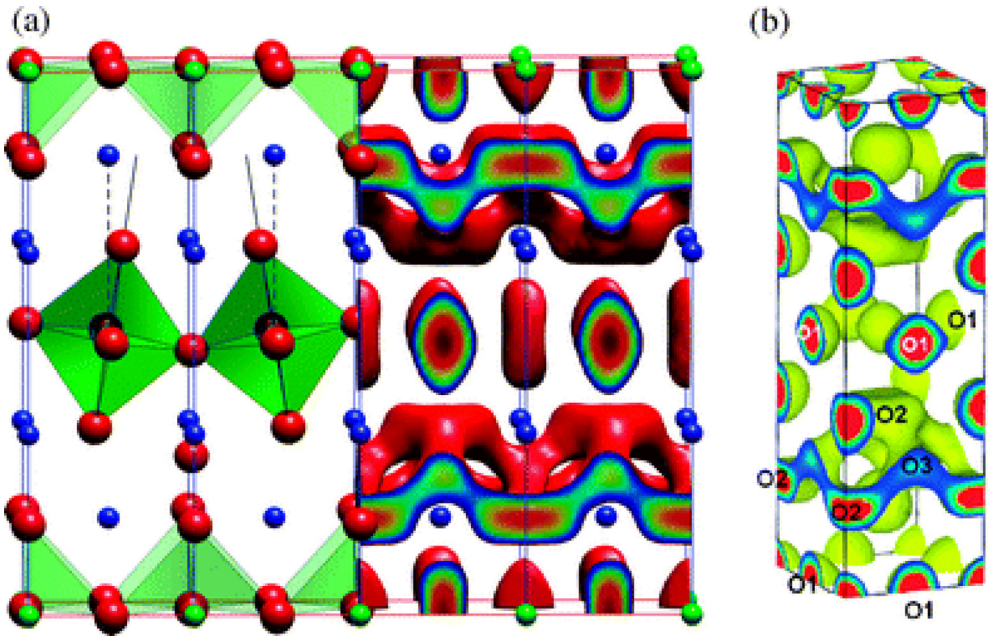

Fig. 5. (a) atomistic simulation interstitialcy pathway mechanism predicted by Parfitt and co-workers on their studies on PNO and (b) later supported by experimental studies on a related composition by Yashima and co-workers (reproduced with permissions from references 30 and 31 respectively).

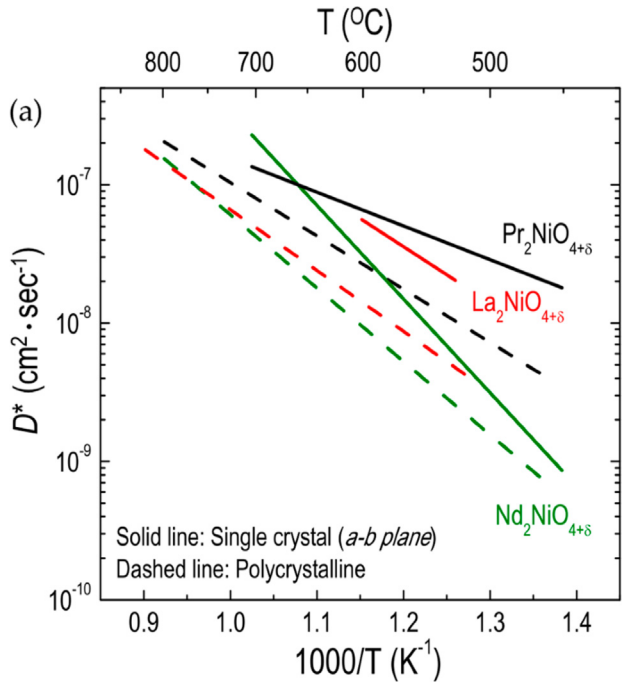

Fig. 7. Diffusion coefficients for nickelates. PNO shows the highest D* and polycrystalline forms of all nickelates show even better D* (adapted from reference [12]).

IT range temperature [20,21]. Bassat and co-workers compared the ionic conductivity of LSCF and LNO and found the ionic conductivity of LNO to be 0.02 Scm^{-1} at 700 °C compared to the 0.003 Scm^{-1} obtained for LSCF at the same temperature [32]. It is possible to manipulate oxygen overstoichiometry – responsible for superior ionic conductivity – by using specific synthetic methods. In the case of an LNO cathode material, δ □□□□□□ ranging from 0.14 to 0.25 have been achieved using reduced temperatures for low δ and oxidation conditions for high δ [14,23,39–44]. Aguadero *et al.* reported $\delta = 0.30$ for LNO, which was expected to enhance the ionic conductivity for the obvious reasons of higher oxygen content (charge carriers) available for transport [44].

In comparison there are very few neutron diffraction studies of lanthanide-based higher-order Ruddlesden-Popper phases (n = 2, 3) such as $La_{0.3}Sr_{2.7}CoFeO_{7-\delta}$ (n = 2), and $LaSr_3Co_{1.5}Fe_{1.5}O_{10-\delta}$ (n = 3) available in the literature [45–47]. Tomkiewicz *et al.* studied both n = 2 and n = 3 Ruddlesden-Popper phases by neutron diffraction and reported the phases crystallised in the tetragonal *I4/mmm* space group. Interestingly, they reported that the oxygen vacancies in these higher-order phases were almost exclusively located within the perovskite layers and only a minimal vacancy formation occurred in the rock-salt layer [47]. This contrasts with our recent studies on n = 3 phase compositions, $LaPr_3Ni_3O_{10-\delta}$ and $LaPr_3Ni_3O_{10-\delta}$ wherein we observe the sizeable presence of vacancies in rock-salt layers, although the majority of vacancies were still located in the perovskite layers [17]. We, however, did observe the large *ab* plane anisotropy of the apical O(4) sites, particularly at high temperatures, indicating faster oxygen diffusion in these materials. This apical oxygen position is indeed known to exhibit an anisotropic Debye-Waller factor and has been widely reported for lower-order Ruddlesden-Popper K_2NiF_4 materials [14,24,48]. Also, our studies further confirmed the strong preference for the curved oxygen transport pathways around the NiO_6 octahedra in these materials [17].

4. Performance and stability

Several studies of the electrochemical performance of the Ruddlesden-Popper phases have been reported in the literature. Amow and Skinner obtained relatively high Area Specific Resistances (ASR) (>1.0 Ω cm^2 at 800 °C) which was improved by Escudero *et al.* who reported an ASR of 0.48 Ω cm^2 at 800 °C for LNO with an $La_{1-x}Sr_xGa_{1-y}Mg_yO_{3-d}$ (LSGM) electrolyte [49]. Aguadero *et al.* substituted the B site cation and obtained the best performance of ASR = 3.7 Ωcm^2 at 850 °C for a Cu doped LNO, significantly higher than reported for the unsubstituted materials [50]. There have been several further attempts to improve the performance of these materials. PNO and NNO, despite their better performance in terms of absolute cell resistance when compared to LNO, suffer from decomposition under operation, which does not bode well for their use as SOFC cathodes [51]. Graded cathodes too have been used to improve the performance of these materials. Rieu and Sayers tested graded LNO cathodes, and they used a compact LNO interlayer between the electrolyte and porous LNO cathode which resulted in a seven-fold drop in ASR from 7.4 Ωcm^2 to 1.0 Ωcm^2 at 700 °C [52,53]. An Arrhenius plot (Fig. 8), compares the performance of these lower-order Ruddlesden-Popper phases with a state-of-the-art LSCF + CGO composite cathode [54]. A recent attempt at improving the performance of these materials by Bassat *et al.* yielded the remarkable performance of 0.030 Ωcm^2 at 700 °C for a PNO cathode [16]. The mixed composition cathodes $La_{2-x}Pr_xNiO_{4+\delta}$ (LPNO) were studied by Vibhu and co-workers and they reported improved performance but observed the decomposition by increasing the Pr content of these mixed La and Pr cathodes [55].

The phase stability of the lower-order phases such as LNO, PNO and NNO materials under operating conditions is the main issue with these materials, which effectively limits their use [16,36,55–58]. Amow *et al.* also reported an ageing study of LNO, and they observed a Ni^{2+}/Ni^{3+} impurity phase after firing the materials for two weeks in the air at 900 °C [36,56,58]. This observation raised concerns about the suitability of LNO as an IT-SOFC cathode. Bassat *et al.* also studied and compared the stability and electrochemical behaviour of Pr-based Ruddlesden-Popper phases as cathodes for IT-SOFCs and observed the decomposition of PNO whereas no such issue was observed in the studies of $Pr_4Ni_3O_{10\pm\delta}$ (P4N3), a higher-order (n = 3) Ruddlesden-Popper series member [16]. They further comment that P4N3 is a very promising cathode material among all three ($PrNiO_{3-\delta}$, PNO and P4N3) Pr-based nickelates (Fig. 9) [16]. This was further confirmed by Vibhu, and co-workers and they reported that the P4N3 material remained stable up to 1000 °C and that the structure retained the orthorhombic *Fmmm* space group symmetry throughout [59].

Ruddlesden-Popper phase materials have been known to react with the YSZ and CGO electrolytes [51,60]. Hernández *et al.* observed the formation of secondary phases such as $La_3Ni_2O_{7-\delta}$, $La_4Ni_3O_{10-\delta}$ (L4N3), $LaNiO_3$ and NiO when used with YSZ or CGO as the electrolyte. They furthermore observed the formation of an insulating pyrochlore phase, $La_2Zr_2O_7$, with a YSZ electrolyte. They comment that the reactivity and formation of insulating phases when using LNO as a cathode with YSZ and CGO electrolytes is the chief drawback for its use [60]. They also observed decomposition of PNO when used with YSZ and CGO as an electrolyte but were not able to confirm whether there was reactivity between the electrode and electrolyte or only decomposition of the PNO electrode [51]. Sayers also confirmed these studies and reported the deleterious reactivity of LNO with a CGO electrolyte but confirmed the suitability of LSGM as an electrolyte with these materials by reporting no reactivity between LSGM and LNO [61].

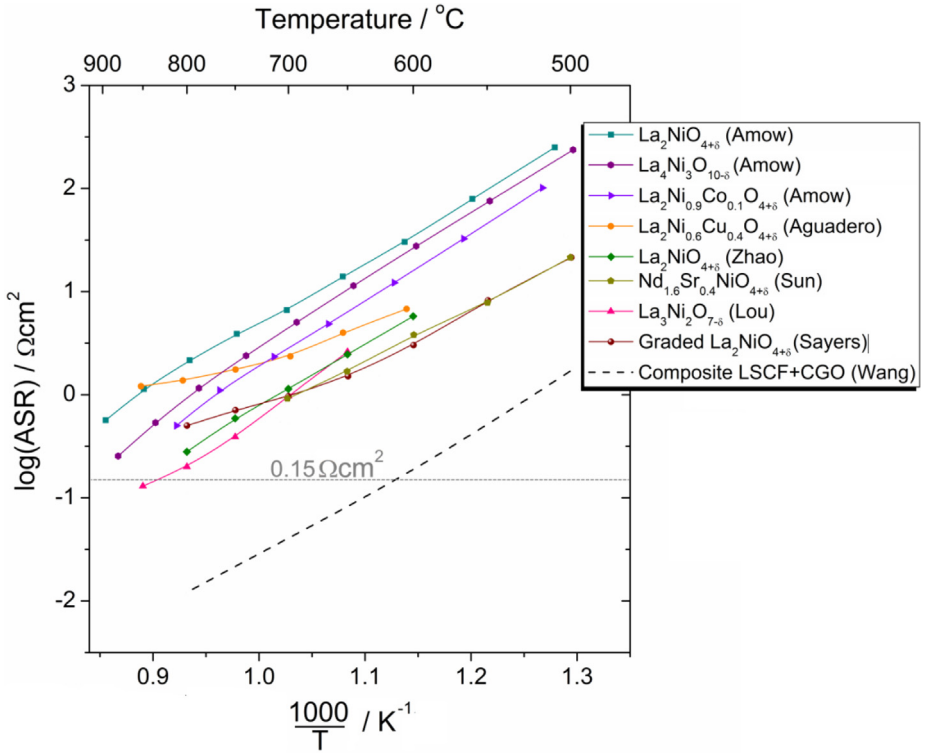

Fig. 8. Log (ASR) vs. 1000/T for various R-P phases, with comparison to state-of-the-art LSCF + CGO composite (adapted from reference [54]).

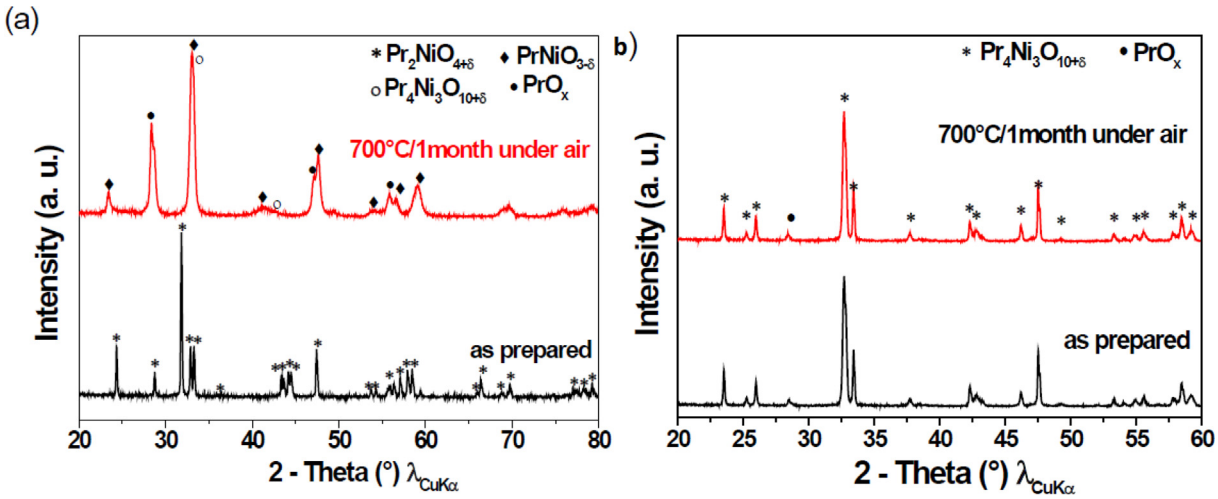

Fig. 9. Ageing studies of (a) PNO and (b P4N3 showing the decomposition of lower-order PNO after heating the sample at 700 °C for one month while as no such decomposition is observed in higher-order P4N3 (reproduced with permission from reference [16]).

These phases, furthermore, are semiconducting in nature and therefore afford limited electronic conductivity [36,56,58]. For example, LNO gives the best results of the electrical conductivity of 70–80 Scm^{-1} in the temperature range of 600–800 °C [56]. They further report a slight increase in these values by doping with Co, however, the electrical conductivity observed still falls short of the ideal value of 100 Scm^{-1}, which has been identified as one of the main reasons behind the reports of high ASR values in these compositions [58].

The impurity Ni^{2+}/Ni^{3+} phase formation at 900 °C in LNO stems from the fact that stoichiometric $La_2NiO_{4+\delta}$ (δ = 0) is mainly comprised of Ni^{2+} ions, while Ni^{3+} is the predominant oxidation state in higher-order phases (n = 2 and 3). As Ni^{2+} tends to oxidise and stabilise the higher-order phases, it is expected that higher-order phases such as $La_4Ni_3O_{9.78}$ (L4N3) and $Pr_4Ni_3O_{10\pm\delta}$ (P4N3) might exhibit increased long-term stability. Indeed, Amow *et al.* did observe that higher-order phases show increased stability and no impurity phase formation [56]. They reported impurity phase formation after heating an n = 1 LNO phase at 900 °C for 2 weeks in air, while no such impurity was observed in the n = 2 and 3 phases after ageing them at 900 °C for 2 weeks in air.

Furthermore, as evidenced by the electrochemical performance studies, it appears that lower electronic conductivity is the main limiting factor in LNO cathodes. PNO and Pr rich lower-order phases, however, do show better electrical conductivity than LNO but because of the severe decomposition observed at 700℃ during

ageing, the use of Pr based lower-order phase materials as IT-SOFC cathodes are severely limited [16,55]. However, higher-order Ruddlesden-Popper phases showed improved electronic conductivity because it has been identified that there are more conduction pathways – that is more NiO_6 corner-sharing octahedra – than lower-order phase materials [56]. Furthermore, it has been shown experimentally by Zhang and Greenblatt that hybridisation of the Ni 3d and O 2p orbitals along the c-direction increases considerably with increasing Ni oxidation state, suggesting higher electrical conductivity as we move towards higher-order phases [62].

Indeed, higher-order Ruddlesden-Popper phases have been reported to possess superior electrical conductivity [36,56,58,62]. Amow et al studied the thermal behaviour of electrical conductivity of these materials and found that the (L4N3) phase is metallic, with electrical conductivity decreasing monotonically as the temperature increases while LNO showed semiconducting behaviour [56]. They observed the electrical conductivity of L4N3 ranging from 110 to 130 Scm^{-1} in the intermediate temperature range (800–600 °C) while the electrical conductivity afforded by LNO in the same temperature range is only around 80 Scm^{-1}. It should also be noted that the samples prepared by Amow *et al.* were of low density and hence likely to underestimate the total conductivity.

Amow and co-workers studied $La_2NiO_{4.15}$ (n = 1), $La_3Ni_2O_{6.95}$ (L3N2; n = 2) and $La_4Ni_3O_{9.78}$ (L4N3; n = 3) and also compared their conductivity, stability, TEC, and ASR in the temperature ranges of interest for solid oxide fuel cell operation [56]. As already mentioned, L4N3 was found to be stable with no impurity formation on heating at 900 °C for 2 weeks. They furthermore found that the TEC of both L3N2 and L4N3 was $\sim 13.2 \times 10^{-6}$ K^{-1}, which is slightly better in terms of compatibility with the commonly used electrolyte and anode materials in SOFCs than the observed TEC of $\sim 13.8 \times 10^{-6}$ K^{-1} for LNO. The ASR, although being higher than the target value of 0.15 Ωcm^2, reflected the increased conductivity as the number of perovskite blocks, n, increased, and thus $La_4Ni_3O_{9.78}$ showed the lowest ASR of 1 Ωcm^2 at 800 °C.

It is well known that microstructure and electrode adherence to the electrolyte can be optimised to realise better performance. In this regard, there are many reports in the literature highlighting the routes to optimise the microstructure and improve the adherence of electrode materials to electrolyte surfaces [54,59,63–65]. Working on ungraded and functionally graded composites of LNO and L4N3, Woolley and Skinner showed the significant role microstructure and electrode/electrolyte contact have on the performance of a material used as an electrode [54,64,65]. They reported the ASR of 0.62 Ωcm^2 at 700 °C for an ungraded 50:50 composite, which was further improved to 0.53 Ωcm^2 at 700 °C by functional grading of the 50:50 composite cathode. This improved performance in both cases was ascribed to a good combination of ionic and total conductivity, being contributed by two different constituents of the composite and the resulting microstructure and improved electrode/electrolyte interface contact.

Several authors working on the related Ruddlesden Popper materials L3N2 and L4N3 have explored the development of the microstructure, including preparing infiltrated composite cathodes of these oxides and reported improvement in the performance results [66–69]. Choi *et al.* reported ASR of 0.11 Ωcm^2 at 750 °C for L3N2 and also confirmed earlier reports of increasing conductivity with increasing *n* [66]. They further reported promising power densities on using L4N3-YSZ composites as a cathode with a YSZ electrolyte; 614, 889, and 1197 mW/cm^2 at 700, 750 and 800 °C respectively. Kim *et al.* doped L4N3 with Sr and reported the ASR of doped-L4N3-YSZ nanocomposite cathode as 0.13 Ωcm^2 at 750 °C [67]. Our group studied $La_2Pr_2Ni_3O_{10-\delta}$, $La_3PrNi_3O_{10-\delta}$ and $LaPr_3Ni_3O_{10-\delta}$ and reported promising performance of these compositions in half-cell mode, with an excellent ASR of 0.08 Ωcm^2 at 700 °C for $LaPr_3Ni_3O_{10-\delta}$ composition [19,70,71].

Sharma and co-workers used a spray deposition technique and improved the performance of L4N3, reporting an ASR of 0.30 Ωcm^2 at 700 °C, with further improvement by one order of magnitude after using the composites with CGO [68,69]. This is a significant improvement in comparison to the earlier reported ASR of 1.0 Ωcm^2 at 800 °C by Munnings *et al.* and has been ascribed to the improvement of cathode microstructure and interface structure [72]. Similarly, Vibhu *et al.* recently reported the promising performance of P4N3 as an oxygen electrode for SOFCs [59]. The chemical stability of the material as reported by Vibhu *et al.* under the conditions of interest was promising [59]. The material was found to be stable at 600 °C, 700 °C and 800 °C for one month, and thus deemed suitable for IT-SOFCs (Fig. 8). The material further showed acceptable TEC of 12×10^{-6} K^{-1} at IT-SOFC operating temperatures and thus met the cathode material requirements. They further reported the electrical conductivity of the material as ranging from 85 to 200 Scm^{-1} from 800 °C to room temperature. The values towards higher temperature are slightly lower but it is important to keep in mind that the reported conductivity values are slightly underestimated as the samples used in this study were only about 70% dense. The study further reports the single-cell performance of this composition with Ni-8YSZ anode; maximum power densities of 1.6 W/cm^2 at 800 °C and 0.68 W/cm^2 at 700 °C.

5. Conclusions

Perovskites such as $La_{1-x}Sr_xMnO_3$ and $La_{1-x}Sr_xCo_{1-y}Fe_yO_{3-d}$, and related oxide materials have received considerable research attention as potential electrode materials for solid oxide fuel cells because of their excellent electrochemical performance. Despite the potential of the LSCF and related materials, there are limitations in terms of stability that have led to further interest in materials of the structurally related Ruddlesden-Popper (RP) family of oxides, $A_{n+1}B_nO_{3n+1}$ where A = Ln, B = transition metal. From early studies of the RP phases, it was evident that their ionic and electronic transport properties indicated that these phases would be promising candidates as SOFC cathodes, but the n = 1 phases such as La_2NiO_4 suffered from lower performance and stability concerns. More recent developments of the n = 2 and 3 phases, and the double perovskites, have shown attractive performance, particularly when the optimisation of the microstructure is considered. Furthermore, these phases may provide routes to new applications such as in co-electrolysis cells, or as potential electrodes in proton-conducting ceramic fuel cells. The are many opportunities to develop the layered perovskite materials, including in the development of composite electrodes for both fuel cell and electrolysis modes of operation. These are an exciting class of materials with considerable potential in a range of devices.

Declaration of Competing Interest

The authors declare that they have no known competing financial interests or personal relationships that could have appeared to influence the work reported in this paper.

Acknowledgements

The authors would like to thank the EU Horizon 2020 (HERMES; Grant No. 952184) for funding this research.

References

[1] J.T.S. Irvine, D. Neagu, M.C. Verbraeken, C. Chatzichristodoulou, C. Graves, M.B. Mogensen, Nat. Energy 1 (2016) 15014.

[2] A. Grimaud, F. Mauvy, J. Marc Bassat, S. Fourcade, M. Marrony, J. Claude Grenier, J. Mater. Chem. 22 (2012) 16017–16025.
[3] L.W. Tai, M.M. Nasrallah, H.U. Anderson, D.M. Sparlin, S.R. Sehlin, Solid State Ionics 76 (1995) 259–271.
[4] Y. Teraoka, H.M. Zhang, K. Okamoto, N. Yamazoe, Mater. Res. Bull. 23 (1988) 51–58.
[5] A.A. Taskin, A.N. Lavrov, Y. Ando, Prog. Solid State Chem. 35 (2007) 481–490.
[6] A.A. Taskin, A.N. Lavrov, Y. Ando, Phys. Rev. B 71 (2005) 134414.
[7] S. Afroze, A. Karim, Q. Cheok, S. Eriksson, A.K. Azad, Front. Energy 13 (2019) 770–797.
[8] P. Kaur, K. Singh, Ceram. Int. 46 (2020) 5521–5535.
[9] S.J. Skinner, Int. J. Inorg. Mater. 3 (2001) 113–121.
[10] S.N. Ruddlesden, P. Popper, Acta Cryst. 11 (54) (1958) 55.
[11] B.v. Beznosikov, K.S. Aleksandrov, Crystallogr. Rep. 45 (2000) 792–798.
[12] D. Lee, H. Lee, Materials 10 (2017) 368.
[13] H. Wilhelm, C. Cros, E. Reny, G. Demazeau, M. Hanfland, J. Solid State Chem. 151 (2000) 231–240.
[14] S.J. Skinner, Solid State Sci. 5 (2003) 419–426.
[15] V. Vibhu, A. Rougier, C. Nicollet, A. Flura, J.C. Grenier, J.M. Bassat, Solid State Ionics 278 (2015) 32–37.
[16] J.-M. Bassat, V. Vibhu, C. Nicollet, A. Flura, S. Fourcade, J.-C. Grenier, A. Rougier, ECS Trans. 78 (2017) 655–665.
[17] M. A. Yatoo, PhD Thesis, Imperial College London, 2019.
[18] C.Y. Tsai, A. Aguadero, S.J. Skinner, J. Solid State Chem. 289 (2020) 121533.
[19] M.A. Yatoo, A. Aguadero, S.J. Skinner, APL Materials, 7, 8.
[20] V.v. Kharton, A.P. Viskup, E.N. Naumovich, F.M.B. Marques, J. Mater. Chem., 9, 2623–2629.
[21] J.A. Kilner, S.J. Skinner, Solid State Ionics 135 (2000) 709–712.
[22] T. Nakamura, R. Oike, Y. Ling, Y. Tamenori, K. Amezawa, PCCP 18 (2016) 1564–1569.
[23] A. Demourgues, A. Wattiaux, J.C. Grenier, M. Pouchard, J.L. Soubeyroux, J.M. Dance, P. Hagenmuller, J. Solid State Chem. 105 (1993) 458–468.
[24] J.D. Jorgensen, B. Dabrowski, S. Pei, D.R. Richards, D.G. Hinks, Phys. Rev. B 40 (1989) 2187–2199.
[25] W. Paulus, A. Cousson, G. Dhalenne, J. Berthon, A. Revcolevschi, S. Hosoya, W. Treutmann, G. Heger, R. Le Toquin, Solid State Sci. 4 (2002) 565–573.
[26] M.S.D. Read, M.S. Islam, G.W. Watson, F.E. Hancock, J. Mater. Chem. 11 (2001) 2597–2602.
[27] L. Minervini, R.W. Grimes, J.A. Kilner, K.E. Sickafus, J. Mater. Chem. 10 (2000) 2349–2354.
[28] C. Frayret, A. Villesuzanne, M. Pouchard, Chem. Mater. 17 (2005) 6538–6544.
[29] L. Yan, H.J. Niu, G.v. Duong, M.R. Suchomel, J. Bacsa, P.R. Chalker, J. Hadermann, G. van Tendeloo, M.J. Rosseinsky, Chem. Sci. 2 (2011) 261–272.
[30] D. Parfitt, A. Chroneos, J.A. Kilner, R.W. Grimes, PCCP 12 (2010) 6834–6836.
[31] M. Yashima, N. Sirikanda, T. Ishihara, J. Am. Chem. Soc. 132 (2010) 2385–2392.
[32] J.M. Bassat, P. Odier, A. Villesuzanne, C. Marin, M. Pouchard, Solid State Ionics 167 (2004) 341–347.
[33] V.V. Kharton, A.P. Viskup, A. Kovalevsky, E.N. Naumovich, F.M.B. Marques, Solid State Ionics 143 (2001) 337–353.
[34] E. Boehm, J.M. Bassat, P. Dordor, F. Mauvy, J.C. Grenier, P. Stevens, Solid State Ionics 176 (2005) 2717–2725.
[35] S.J. Skinner, J.A. Kilner, Ionics 5 (1999) 171–174.
[36] G. Amow, I. Davidson, S. Skinner, Proceedings of the Electrochemical Society SOFC-IX (2005) 1745.
[37] J.M. Bassat, M. Burriel, M. Ceretti, P. Veber, J.C. Grenier, W. Paulus, J.A. Kilner, Solid Oxide Fuel Cells 13 (Sofc-Xiii) 57 (2013) 1753–1760.
[38] A. Aguadero, L. Fawcett, S. Taub, R. Woolley, K.-T. Wu, N. Xu, J.A. Kilner, S.J. Skinner, J. Mater. Sci. 47 (2012) 3925–3948.
[39] A. Petric, P. Huang, F. Tietz, Solid State Ionics 135 (2000) 719–725.
[40] E.N. Naumovich, M.V. Patrakeev, V.V. Kharton, A.A. Yaremchenko, D.I. Logvinovich, F.M.B. Marques, Solid State Sci. 7 (2005) 1353–1362.
[41] E. Boehm, J.M. Bassat, M.C. Steil, P. Dordor, F. Mauvy, J.C. Grenier, Solid State Sci. 5 (2003) 973–981.
[42] J.M. Bassat, P. Odier, J.P. Loup, J. Solid State Chem. 110 (1994) 124–135.
[43] P. Odier, J.M. Bassat, J.C. Rifflet, J.P. Loup, Solid State Commun. 85 (1993) 561–564.
[44] A. Aguadero, J.A. Alonso, M.J. Martinez-Lope, M.T. Fernandez-Diaz, M.J. Escudero, L. Daza, J. Mater. Chem. 16 (2006) 3402–3408.
[45] M.A. Tamimi, S. McIntosh, J. Mater. Chem. A 2 (2014) 6015–6026.
[46] A.C. Tomkiewicz, M.A. Tamimi, A. Huq, S. McIntosh, Faraday Discuss. 182 (2015) 113–127.
[47] A.C. Tomkiewicz, M. Tamimi, A. Huq, S. McIntosh, J. Mater. Chem. A 3 (2015) 21864–21874.
[48] J.D.J.T. Egami. Dmowski D.G. Hinks, D.W. Capone II, C.U. Segre, K. Zhang, Reviews of Solid State Science, 1, 11.
[49] M.J. Escudero, A. Fuerte, L. Daza, J. Power Sources 196 (2011) 7245–7250.
[50] A. Aguadero, J.A. Alonso, M.J. Escudero, L. Daza, Solid State Ionics 179 (2008) 393–400.
[51] A. Montenegro-Hernández, J. Vega-Castillo, L. Mogni, A. Caneiro, Int. J. Hydrogen Energy 36 (2011) 15704–15714.
[52] M. Rieu, R. Sayers, M.A. Laguna-Bercero, S.J. Skinner, P. Lenormand, F. Ansart, J. Electrochem. Soc. 157 (2010) B477–B480.
[53] R. Sayers, M. Rieu, P. Lenormand, F. Ansart, J.A. Kilner, S.J. Skinner, Solid State Ionics 192 (2011) 531–534.
[54] Russell Woolley, PhD Thesis, Imperial College London, 2013.
[55] V. Vibhu, J.-M. Bassat, A. Flura, C. Nicollet, J.-C. Grenier, A. Rougier, ECS Trans. 68 (2015) 825–835.
[56] G. Amow, I. Davidson, S. Skinner, Solid State Ionics 177 (2006) 1205–1210.
[57] G. Amow, P.S. Whitfield, I.J. Davidson, R.P. Hammond, C.N. Munnings, S.J. Skinner, Ceram. Int. 30 (2004) 1635–1639.
[58] G. Amow, S.J. Skinner, J. Solid State Electrochem. 10 (2006) 538–546.
[59] V. Vibhu, A. Rougier, C. Nicollet, A. Flura, S. Fourcade, N. Penin, J.-C. Grenier, J.-M. Bassat, J. Power Sources 317 (2016) 184–193.
[60] A.M. Hernández, L. Mogni, A. Caneiro, Int. J. Hydrogen Energy 35 (2010) 6031–6036.
[61] R. Sayers, J. Liu, B. Rustumji, S.J. Skinner, Fuel Cells 8 (2008) 338–343.
[62] Z. Zhang, M. Greenblatt, J. Solid State Chem. 117 (1995) 236–246.
[63] C. Ferchaud, J.-C. Grenier, Y. Zhang-Steenwinkel, M.M.A. van Tuel, F.P.F. van Berkel, J.-M. Bassat, J. Power Sources 196 (2011) 1872–1879.
[64] R.J. Woolley, S.J. Skinner, Solid State Ionics 255 (2014) 1–5.
[65] R.J. Woolley, S.J. Skinner, J. Power Sources 243 (2013) 790–795.
[66] S. Choi, S. Yoo, J.-Y. Shin, G. Kim, J. Electrochem. Soc. 158 (2011) B995–B999.
[67] S. Kim, S. Choi, A. Jun, J. Shin, G. Kim, J. Electrochem. Soc. 161 (2014) F1468–F1473.
[68] R.K. Sharma, M. Burriel, L. Dessemond, J.-M. Bassat, E. Djurado, J. Power Sources 325 (2016) 337–345.
[69] R.K. Sharma, M. Burriel, E. Djurado, J. Mater. Chem. A 3 (2015) 23833–23843.
[70] M.A. Yatoo, Z. Du, H. Zhao, A. Aguadero, S.J. Skinner, Solid State Ionics 320 (2018) 148–151.
[71] M.A. Yatoo, Z. Du, Z. Yang, H. Zhao, S.J. Skinner, , DOI:10.3390/cryst10060428.
[72] C. Munnings, S. Skinner, G. Amow, P. Whitfield, I. Davidson, Solid State Ionics 177 (2006) 1849–1853.